

## Supporting Information

### **(Kunkeaw, et al: “A novel mechanism mediated by a non-coding RNA, nc886, in the cytotoxicity of a DNA-reactive compound”)**

#### **Materials and Methods**

##### *Cell lines, antibodies, and other reagents*

All cell lines, antibodies, and other reagents are described in (1-3), unless otherwise specified below. Huh7.5 cell line is our laboratory stock. Doxorubicin, etoposide, and aclarubicin were purchased from EMD Millipore (Billerica, MA), Sigma-Aldrich (St. Louis, MO), and Santa Cruz Biotechnology (Dallas, TX) respectively. H<sub>2</sub>O<sub>2</sub> and deferoxamine mesylate were from Fisher Chemical (Waltham, MA) and Sigma-Aldrich respectively. Antibodies against total p53 and Chk2 were purchased from Santa Cruz Biotechnology and those against their phospho forms were from Cell Signaling Technology (Danvers, MA).

##### *Primers, plasmid DNAs, RNAs, and transfection*

Sequences for PCR primers and Northern probes are summarized in SI Appendix, Dataset S4. The nc886-expressing DNA was a PCR-amplified 649 nt PCR fragment containing the 101 nt nc886 transcript and flanking sequences (271 nt and 277 nt at the 5'- and 3'-side respectively). This fragment was inserted into the pCR4-TOPO vector (Invitrogen, Carlsbad, CA). The resultant plasmid and the PCR fragment were used in transfection experiments in Fig S17. For NF- $\kappa$ B luciferase assays, pNF- $\kappa$ B-Luc (Stratagene, La Jolla, CA) was co-transfected with pRL-SV40 (Promega, Madison, WI) for normalization. siRNAs directed against PKR and MVP were Stealth RNAi™ siRNA (Invitrogen). Three siRNAs targeting different regions of a gene (whose sequences are available upon request) were equally mixed and transfected at 40 nM. Anti-oligos directed against nc886 and canonical

vtRNAs (vtRNA1-1, 1-2, 1-3) were DNA-RNA mix-mer with a modified sugar (2'-O-methoxy) and a phosphorothioate backbone as described in (1) and their targeting sequence are 5'-aucucugugcuggguucga-3' (corresponding nt 56-75 of nc886) and 5'-ggcuggcuuuagcucagcgg-3' (corresponding nt 2-21 of vtRNAs). These anti-oligos were transfected at 200 nM. For the rescue experiments (Fig 2E-H and S8-9), *in vitro* transcribed nc886 and vtRNAs were prepared as described in (2) and yeast tRNA was purchased from Applied Biosystems/Ambion (Carlsbad, CA). Short RNAs (siRNAs, anti-oligos, and *in vitro* transcripts) were transfected with Lipofectamine™ RNAiMAX reagent (Invitrogen) and DNAs were transfected with Lipofectamine™ 2000 reagent (Invitrogen).

#### ***Luciferase assays, and cell proliferation assays, and in vitro kinase assays***

All these assays were performed as described in (1, 2).

#### ***fCLIP-PCR***

PKR-nc886 interaction was analyzed using formaldehyde-crosslinking and immunoprecipitation followed by qRT-PCR (fCLIP-PCR) approach as described in (4). Cells were fixed with 0.1% paraformaldehyde (Sigma-Aldrich) at room temperature (RT) for 10 min. Glycine was added immediately to the solution and incubated for additional 10 min to quench the reaction. Cells were then lysed in the fCLIP lysis buffer [20 mM Tris-HCl (pH 7.5), 15 mM NaCl, 10 mM EDTA, 0.5% Nonidet P-40, 0.1% Triton X-100, 0.1% sodium dodecyl sulfate (SDS), 0.1% sodium deoxycholate supplemented with protease and RNase inhibitors] and sonicated 3 times, 5 min each. The sodium concentration was adjusted to 150 mM and lysate was centrifuged at maximum speed for 15 min to remove debris and insoluble fraction. The lysate was immunoprecipitated using PKR antibody (#12297 from Cell Signaling Technology) attached on protein A agarose beads (Thermo Fisher Scientific, Waltham, MA) for 3 hr at 4 °C. Beads were then washed 3 times with the fCLIP wash buffer [20 mM Tris-HCl (pH 7.5), 15 mM NaCl, 10 mM EDTA, 0.1% Nonidet P-40, 0.1% Triton X-100, 0.1% SDS, 0.1% sodium deoxycholate] and PKR-RNA complexes were eluted by

incubating in the urea elution buffer [200 mM Tris-HCl (pH 7.4), 100 mM NaCl, 20 mM EDTA, 2% SDS, and 7 M Urea) for 3 hr at 25 °C. RNA was then de-crosslinked and separated from PKR by adding 20 mg/ml Proteinase K (Sigma-Aldrich) and incubating at 65 °C for overnight.

RNA was extracted using acid-phenol chloroform and treated with DNase I (TaKaRa Bio Inc., Shiga, Japan) for 30 min to remove genomic DNA. cDNA was synthesized using SuperScript IV Reverse Transcriptase (Thermo Fisher Scientific) with random hexamer primers and analyzed using AriaMx Real-Time PCR (Agilent, Santa Clara, CA). Sequences of PCR primers are listed in SI Appendix, Dataset S4.

### ***Subcellular fractionation***

Subcellular fractionation was performed as described in (1, 5) with modifications. Harvested cells ( $\sim 5 \times 10^7$ ) were resuspended in 1.2 ml of buffer A [50 mM Tris-HCl (pH 7.4), 1.5 mM MgCl<sub>2</sub>, 75 mM NaCl, 0.5% Nonidet P-40] containing 1 mM phenylmethylsulfonyl fluoride, 0.1 ml of protease inhibitor cocktail (GenDepot, Barker, TX), 10 mM ribonucleoside-vanadyl complex (New England Biolabs, Ipswich, MA), and 200 unit/ml RNase inhibitor from human placenta (New England Biolabs). All subsequent steps were performed at 4°C. Resuspended cells were lysed for 10 min and centrifuged at  $6,000 \times g$  for 10 min in a TLA-55 rotor using Optima™ TLX ultracentrifuge (Beckman Coulter, Brea, CA). The pellet was the nuclear fraction (designated “P10” in Fig S10). The supernatant was the bulk cytoplasm and further fractionated by centrifugation at  $100,000 \times g$  for 1 hr, separating the resulting supernatant (designated “S100”) from the pellet (designated “P100”). The P10 and P100 fractions were resuspended with Trizol reagent (Invitrogen) for subsequent RNA preparation or with RIPA buffer for Western blotting. The S100 fraction was concentrated by adding an equal volume of isopropanol followed by centrifugation (12 krpm for 10 min). The resultant pellet was subjected to RNA preparation by Trizol reagent. An aliquot of the S100 fraction was directly loaded for Western blotting.

### ***POLR3A ChIP followed by high-throughput sequencing and PCR (ChIP-seq and –PCR)***

ChIP assays were performed as described previously (6) with minor modifications. Briefly, cells were cross-linked with 1% formaldehyde, incubated in a swelling buffer [5 mM PIPES (pH 8.0), 85 mM KCl, 0.5% Nonidet P-40], and subjected to sonication in buffer A' [10 mM Tris-HCl (pH 8.0), 2 mM EDTA, 0.2% SDS] using Bioruptor (Diagenode, Denville, NJ). Chromatin samples were diluted in buffer B' [10 mM Tris-HCl (pH 8.0), 2% Triton X-100, 280 mM NaCl, 0.2% deoxycholate] and immunoprecipitated with antibodies directed against POLR3A (ab96328 from Abcam, Cambridge, MA). Chromatin-antibody complexes were pulled down by Protein A/G Dynabeads (Invitrogen). After treating with proteinase K and reversing the cross-link, the ChIP-DNA was subjected to high-throughput sequencing and PCR. ChIP-seq run and subsequent analysis were done as previously described (7). ChIP-PCR was performed also as in (7) with primers listed in SI Appendix, Dataset S4.

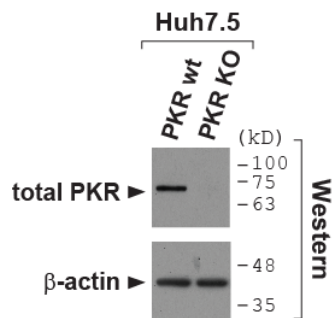
### ***3-D cell culture***

The 3-D cell culture was performed using BiO Assay™ kit from n3D Biosciences (Houston, TX) according to manufacturer's instructions. Briefly,  $3.3 \times 10^6$  cells in monolayer culture were treated with 200  $\mu$ l of NanoShuttle™-PL for 16 hr, trypsinized, and subject to magnetic levitation in a 6-well for 24 hr. The levitated cells were suspended in 2 ml of the culture medium (per a 6-well), resuspended by pipetting, bio-printed onto several 96-wells ( $2.0 \times 10^5$  cells per a 96-well) on the ring drive for 30 min, and then treated with doxorubicin. A brief workflow with schematic and actual images is shown in Fig 4C.

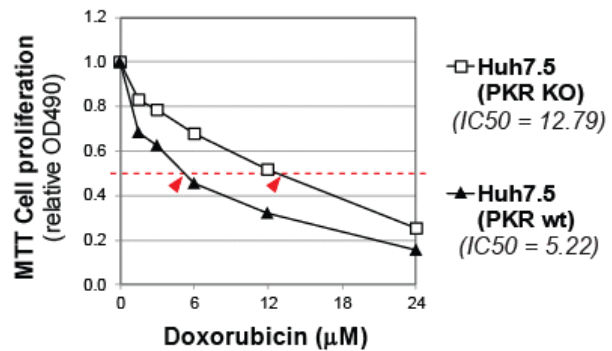
## **Supplementary Figures 1-20**

Figure S1

A



B



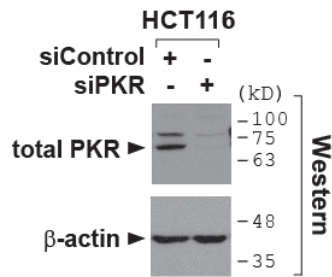
**CRISPR-Cas knockout (KO) of PKR confers doxorubicin resistance on Huh7.5 cells**

**A.** Western blot of PKR to assure PKR KO cells, with  $\beta$ -actin as a loading control. Molecular size markers in kiloDalton (kD) are indicated on the right.

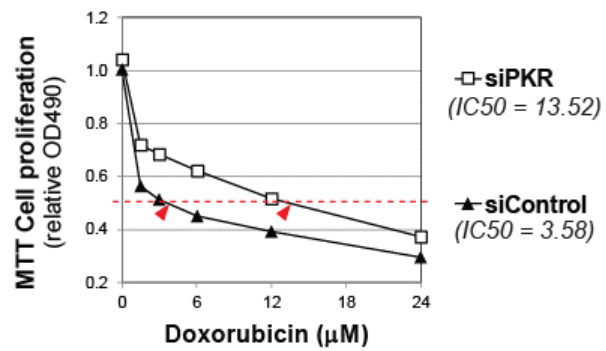
**B.** MTT cell proliferation assays with titrating amounts of doxorubicin. Doxorubicin was treated for 24 hr. The IC<sub>50</sub> values are indicated below each cell line. Each value is an average of triplicate samples. Standard deviations are not shown for simplicity of the plot, because they are small (ranging 0.004 – 0.032) and obscured by markers in most data points.

Figure S2

A



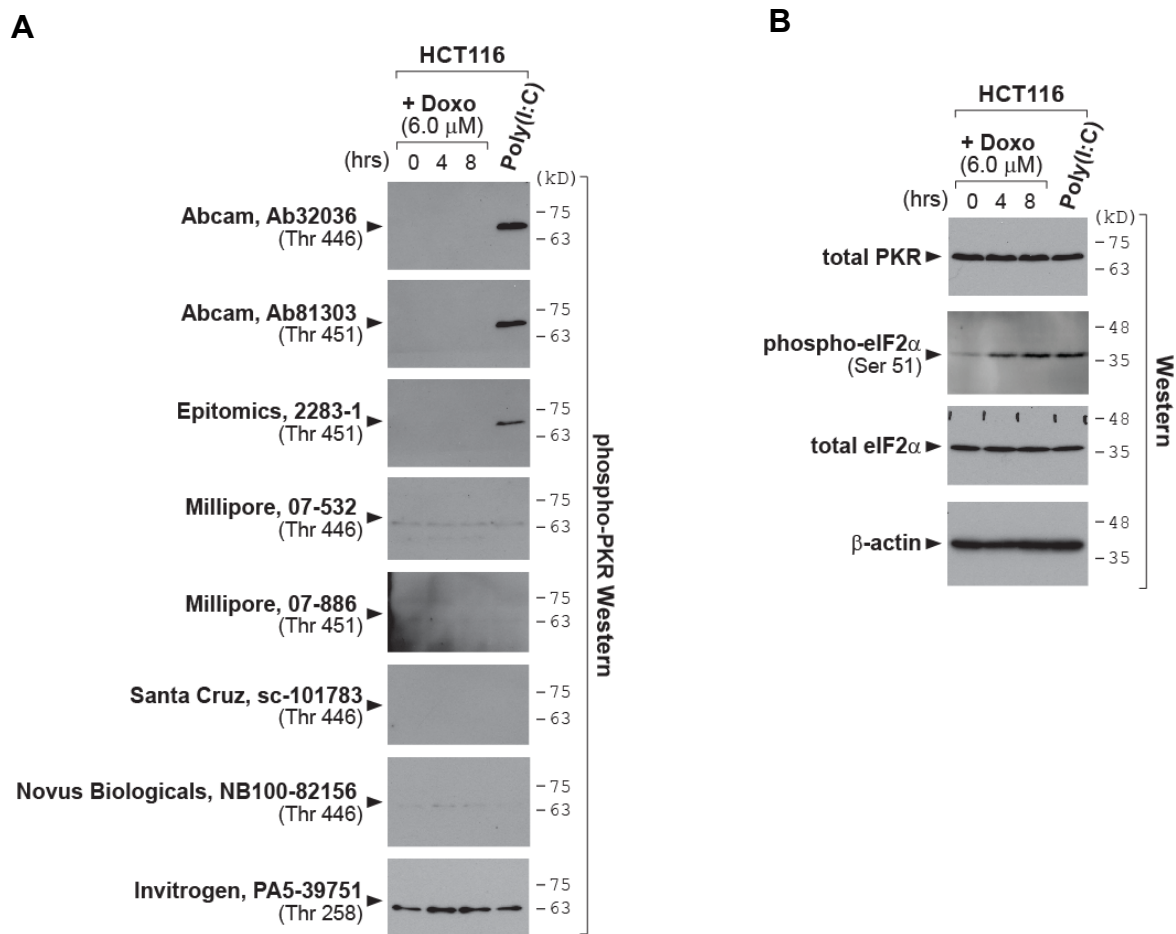
B



**Small interfering RNA (siRNA)-mediated knockdown (KD) of PKR makes HCT116 cells more resistant to doxorubicin**

**A-B.** siRNA was transfected for 48 hr, which was followed by cell harvest for Western blot (panel A) and then doxorubicin treatment for 24 hr and MTT assays (panel B). The range of standard deviation of data points is 0.008-0.025. All other descriptions are the same as Fig S1.

**Figure S3**



### Western blot of phospho-PKR with antibodies from various sources

**A-B.** Western blot of indicated proteins. HCT116 cells were treated with doxorubicin (Doxo) or with Poly(I:C)-LMW (Invivogen; San Diego, CA). Poly(I:C)-LMW was transfected at 1 μg/ml with Lipofectamine™ 2000 reagent for 8 hrs. All Western blots in this figure were done with the same batch of cell lysates.

PKR was activated upon doxorubicin treatment, as shown convincingly by our experimental evidence (phospho-eIF2α Western blot, NF-κB luciferase assays, and *in vitro* kinase assays in Fig 1C-G), except for phospho-PKR Western data. When activated, PKR is auto-phosphorylated at multiple residues including Thr446. Although Western blot of phospho-Thr446 is the most commonly measured indicator for PKR activation, we consistently failed to see the induction of phospho-Thr446 by doxorubicin (Fig 1A and C, see also Fig S14).

It appears that other researchers also experienced this problem. Although a number of reports have established a role for PKR in the doxorubicin-mediated cytotoxicity, whether PKR is genuinely activated has been argued because of unclear or even conflicting results about phospho-PKR Western in several studies (8-13). Some reports did not show a phospho-PKR Western blot (8, 9). Some other reports showed a phospho-PKR Western blot, but the extent of induction was very marginal (10, 11). A significant increase of phospho-PKR in

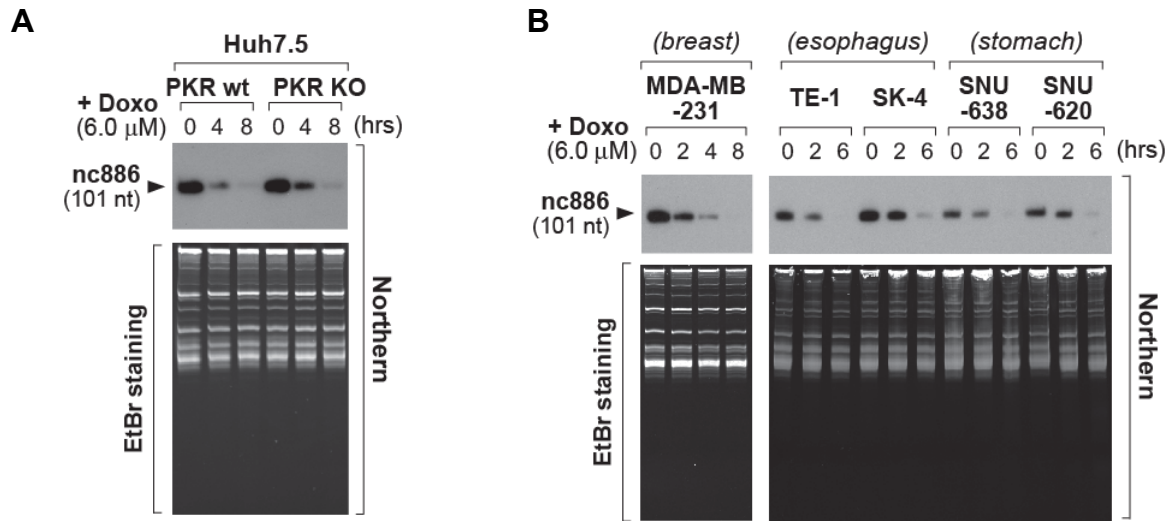
HCT116 cells was seen in one paper (12), but total PKR was also equally increased so that genuine net increase of phospho-PKR was questionable. Furthermore, another paper clearly showed that phospho-PKR (and also total PKR) was not altered by doxorubicin in the same HCT116 cell line (13), in agreement with our data. We wanted to elucidate this issue, by testing several different antibodies against phospho-PKR (panel A) and having included a sample transfected with Poly(I:C), a well-known PKR activator, as a positive control (lane 4).

One of the most widely used antibodies against phospho-PKR is from Abcam (cat # ab32036), which we had used in all our previous studies (1, 2, 14, 15) and throughout this study. We could see a band at the correct size in main figures (Fig 1A and C), but this band became visible only after extended exposure (> 20 min) and, importantly, was not increased by doxorubicin. In the Western blot shown here, we detected the phospho-PKR band only in the Poly(I:C)-treated sample (top blot in panel A) readily upon short exposure (usually < 3 min in the same assay condition). These data assured that our experimental condition for Western blot was appropriate and indicated that the bands in main figures (Fig 1A and C) were an overexposure artifact. Doxorubicin treatment induced phospho-eIF2 $\alpha$  reproducibly in this figure and other figures (compare panel B to Fig 1C and S14) and the extent of induction was comparable to that of Poly(I:C) (compare lanes 2-4 in panel B), indicating doxorubicin activated PKR as efficiently as Poly(I:C).

We suspected whether this puzzling result was a peculiar phenomenon specific to the antibody (ab32036, Abcam) we used. So, we tested other antibodies recognizing Thr446, Thr451, or Thr 258 from various suppliers. Out of seven antibodies, two yielded a similar result to the Abcam ab32036 (top three blots in panel A). The other five antibodies did not detect a correct band in our experimental condition.

We conclude that Western blot of phospho-PKR is almost infeasible with currently available antibodies in the context of doxorubicin treatment. Although Thr446 and Thr451 are typical phosphorylation sites, phosphorylation at these residues might not have occurred upon doxorubicin treatment despite PKR activation. Alternative possibility is that doxorubicin treatment somehow interfered with antibody recognition of phospho-Thr446 (or -Thr451) during Western blot. We prefer the latter possibility, because our *in vitro* kinase assay proved that PKR was genuinely phosphorylated (Fig 1E-F). Although we do not know the underlying reason, this phenomenon demonstrates a complication in PKR detection and cites a caveat that PKR activity should be carefully assessed, when necessary, by *in vitro* kinase assays rather than relying on Western blot analysis for phosphorylation at a single residue.

**Figure S4**

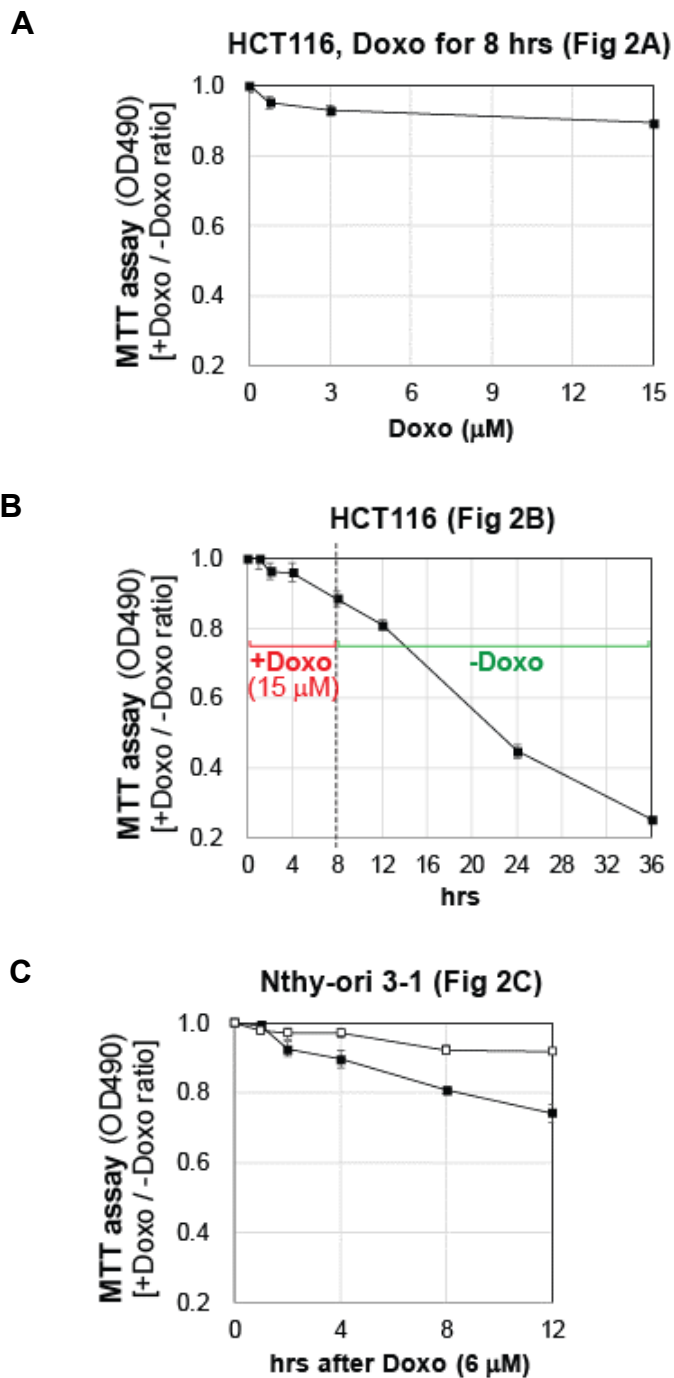


**The expression of nc886 diminishes upon doxorubicin treatment**

**A-B.** Northern blot of nc886 and EtBr staining for a loading control. Doxorubicin treatment conditions are displayed in figure captions.

Besides a colon cancer cell line (HCT116 in Fig 2A-B) and a thyroid cell line (Nthy-ori 3-1 in Fig 2C), we treated doxorubicin in several other cell lines and observed nc886 diminution in all of them; Huh7.5 PKR wt and KO cell lines (panel A), a breast cancer cell line MDA-MB-231, esophageal squamous cell carcinoma and adenocarcinoma cell lines (TE-1 and SK-4 respectively), gastric cancer cell lines SNU-638 and SNU-620 (panel B), and a lung cell line (to be shown in Fig S6).

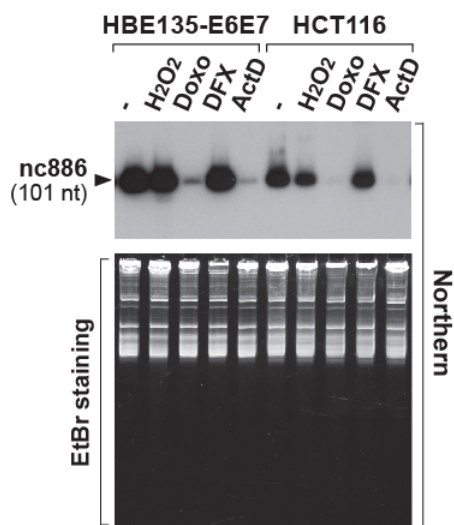
Figure S5



**MTT cell proliferation assays after doxorubicin treatment (for Fig 2A-C).**

Cells were treated with doxorubicin for indicated durations or at indicated concentrations, exactly as in main Fig 2A, 2B, and 2C. At each time point, the other set without doxorubicin treatment was prepared in parallel. After MTT reaction, OD490 values were measured from samples with doxorubicin or without doxorubicin. The ratio (“+Doxo / -Doxo ratio” on y-axis) was calculated and plotted. Each value is an average of tetraplicate samples and the standard error is indicated. The decrease of MTT values was evident but not so robust until 8 hrs.

**Figure S6**

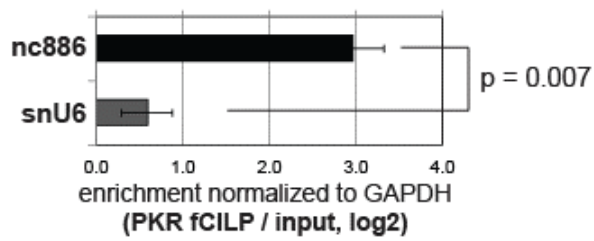


**nc886 diminution is not a simply end result of any stress condition**

Northern blot of nc886 and EtBr staining after 8 hr treatment of indicated cell lines with H<sub>2</sub>O<sub>2</sub> (0.5 mM), doxorubicin (Doxo; 6 μM), desferrioxamine (DFX; 100 μM) and actinomycin D (ActD; 2 μg/ml). Lanes 1 and 6 are no treatment control (designated “-”). HBE135-E6E7 is a transformed lung epithelial cell line.

In contrast to doxorubicin, H<sub>2</sub>O<sub>2</sub> (an oxidative stress inducer) and desferrioxamine (a hypoxia mimetic compound) barely affected nc886. Actinomycin D, a transcription inhibitor included for comparison, inhibited nc886 expression as expected.

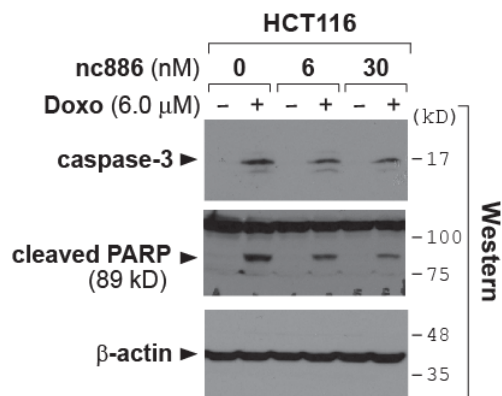
**Figure S7**



**Physical interaction between nc886 and PKR**

*formaldehyde-CrossLinking and ImmunoPrecipitation* followed by qRT-PCR (fCLIP-PCR) of nc886 and U6 small nuclear RNA (snU6) in HCT116 cells. The signal ( $2^{-\Delta\Delta C_t}$  values) of PKR IP was normalized to input and then again normalized to GAPDH (the degree of PKR binding; x-axis).

**Figure S8**

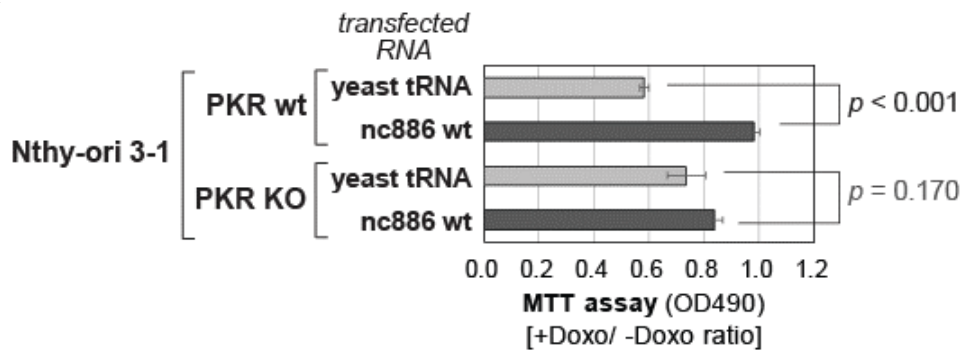


**Attenuation of doxorubicin cytotoxicity by introducing *in vitro* transcribed nc886**

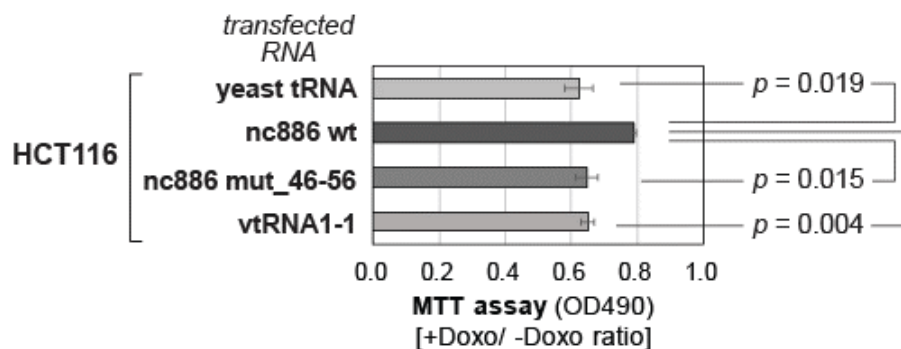
Transfection of the nc886 RNA (an *in vitro* transcript) and treatment were done simultaneously before harvesting cells at 12 hr for Western blot. Each transfection was adjusted to contain the same total μg amount of RNA by adding yeast tRNA to 4 μg (which is equivalent to 30 nM of nc886) in the transfection mixture for a 6-cm dish.

Figure S9

A



B

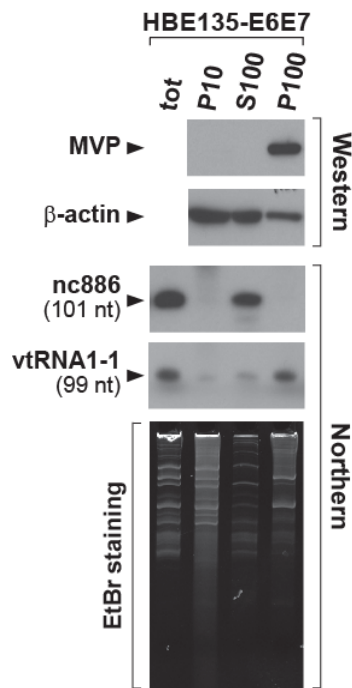


**MTT cell proliferation assays after doxorubicin treatment in combination with transfection of *in vitro* transcribed RNAs (raw data for Fig 2E-H).**

Experiments were performed as described in Fig 2E-H, unless otherwise specified. nc886 (wt or mut\_46-56) or vtRNA1-1 at 15 nM or the equivalent gram amount of yeast tRNA (49 ng per a well in a 96-well plate) was transfected. Transfection and doxorubicin treatment were done simultaneously before MTT assays at 12 hr. Each value is a ratio of OD490 values from +doxorubicin and -doxorubicin samples. An average of tetraplicate samples and the standard error is plotted, with p-values calculated from one-tailed t-test.

nc886 attenuated the doxorubicin toxicity as compared to its mutant form, vtRNA1-1, and yeast tRNA, all of which are deficient at PKR binding. These MTT data corroborated the Western data for apoptotic markers in main figures (panels A and B correspond to Fig 2E and G-H, respectively)

**Figure S10**

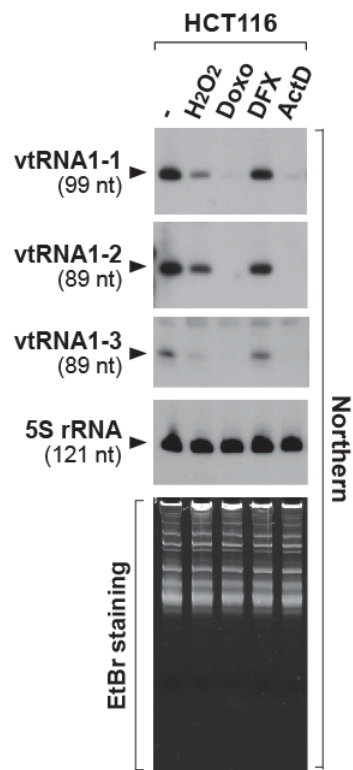


**nc886 is not physically associated with the vault complex**

Subcellular fractionation. Tot, total cells; P10, nuclear fraction; S100, soluble cytoplasmic fraction; P100, cytoplasmic pellet. After fractionation, the same portion of each fraction was loaded for Northern and Western blots.

nc886 is classified as a paralog of vault RNAs (vtRNAs) and one of its aliases is vtRNA2-1 (16). Canonical vtRNAs (vtRNA1-1, 1-2, and 1-3) are constituents of a large ribonucleoprotein complex called the vault complex that has been implicated in drug resistance of cancer cells [reviewed in (17)]. Therefore, we examined whether nc886 exists in the vault complex. We separated the nuclear fraction (“P10”) and the soluble cytoplasmic fraction (“S100”) from the insoluble cytoplasmic pellet (“P100”) which contains large complexes such as ribosomes and vault particles. The major constituent of the vault complex (Major Vault Protein; MVP) was exclusively present in P100. vtRNA1-1 was also enriched in P100, but nc886 was present only in S100 but not in P100. Our data showed that nc886 is not physically associated with the vault complex, in agreement with our previous report (1).

**Figure S11**

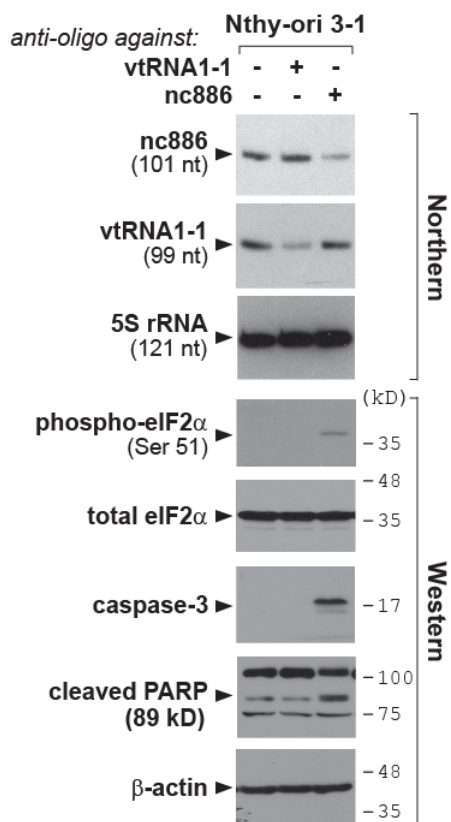


**The expression of canonical vtRNAs is decreased by doxorubicin**

Northern blot of canonical vtRNAs, as done the same as Fig S6.

All three canonical vtRNAs are Pol III transcripts and were decreased by doxorubicin, like nc886. Of note, in case of other stress conditions, the expression pattern of nc886 was different from those of the canonical vtRNAs; for example, nc886 was barely affected by H<sub>2</sub>O<sub>2</sub> (Fig S6) but all three vtRNAs were clearly decreased.

**Figure S12**

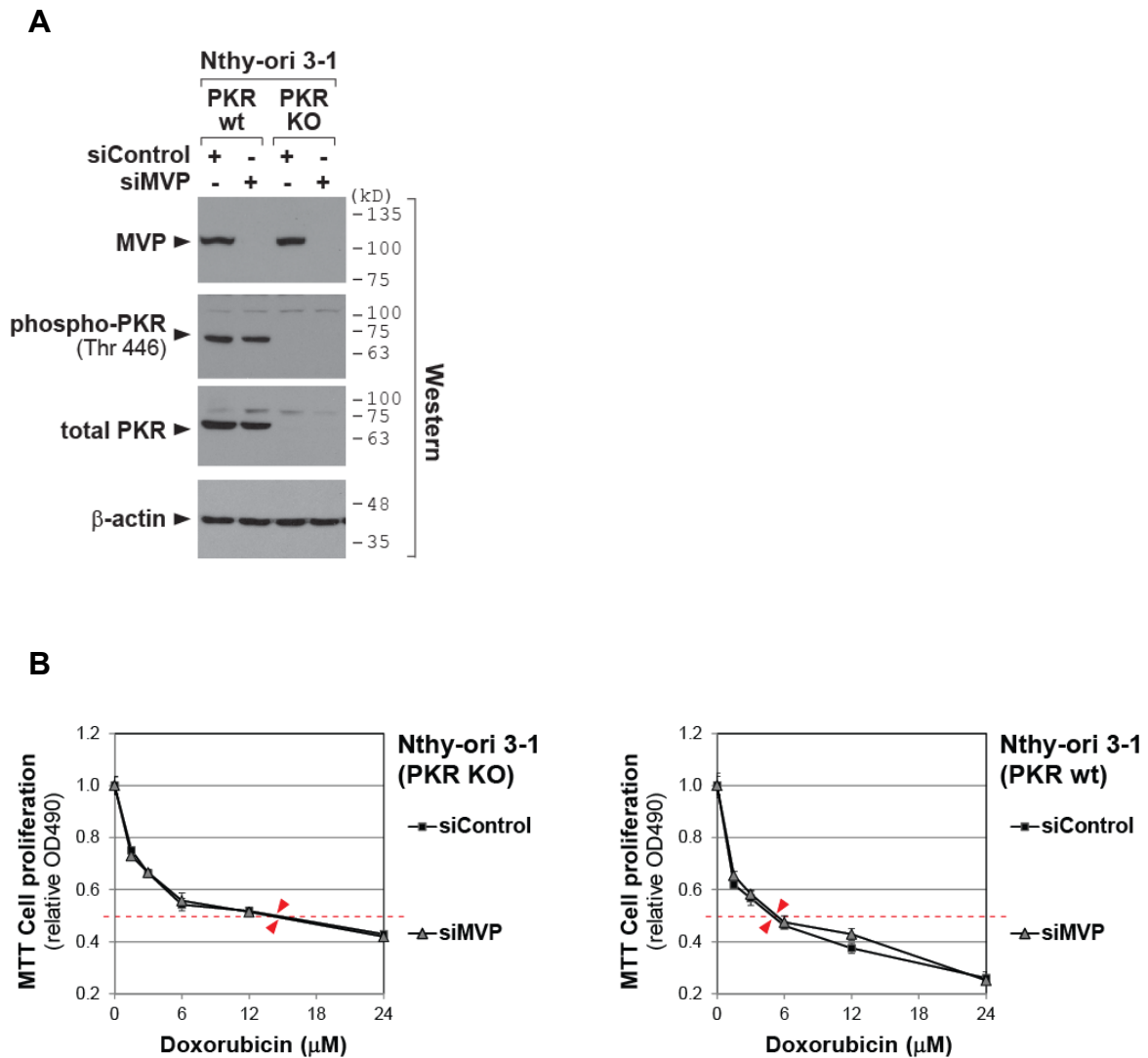


**The KD of vtRNA1-1 did not provoke the PKR-mediated cell death pathway.**

Northern and Western blots at 24 hr after transfection of indicated anti-oligos.

In Fig S11 (and Fig S16 to be shown later), we found all three canonical vtRNAs to be suppressed by doxorubicin, with a similar time course and degree to nc886. This raises a possibility that canonical vtRNAs play a certain role in doxorubicin cytotoxicity independently from nc886. This possibility was checked by KD of vtRNA1-1, which is a canonical vtRNA and was genuinely in physical association with the vault complex (Fig S10). Transfection of an anti-oligo efficiently suppressed vtRNA1-1, but neither activated PKR (as indicated by no phospho-eIF2 $\alpha$ ) nor induced apoptosis (as indicated by caspase-3 and cleaved PARP).

**Figure S13**

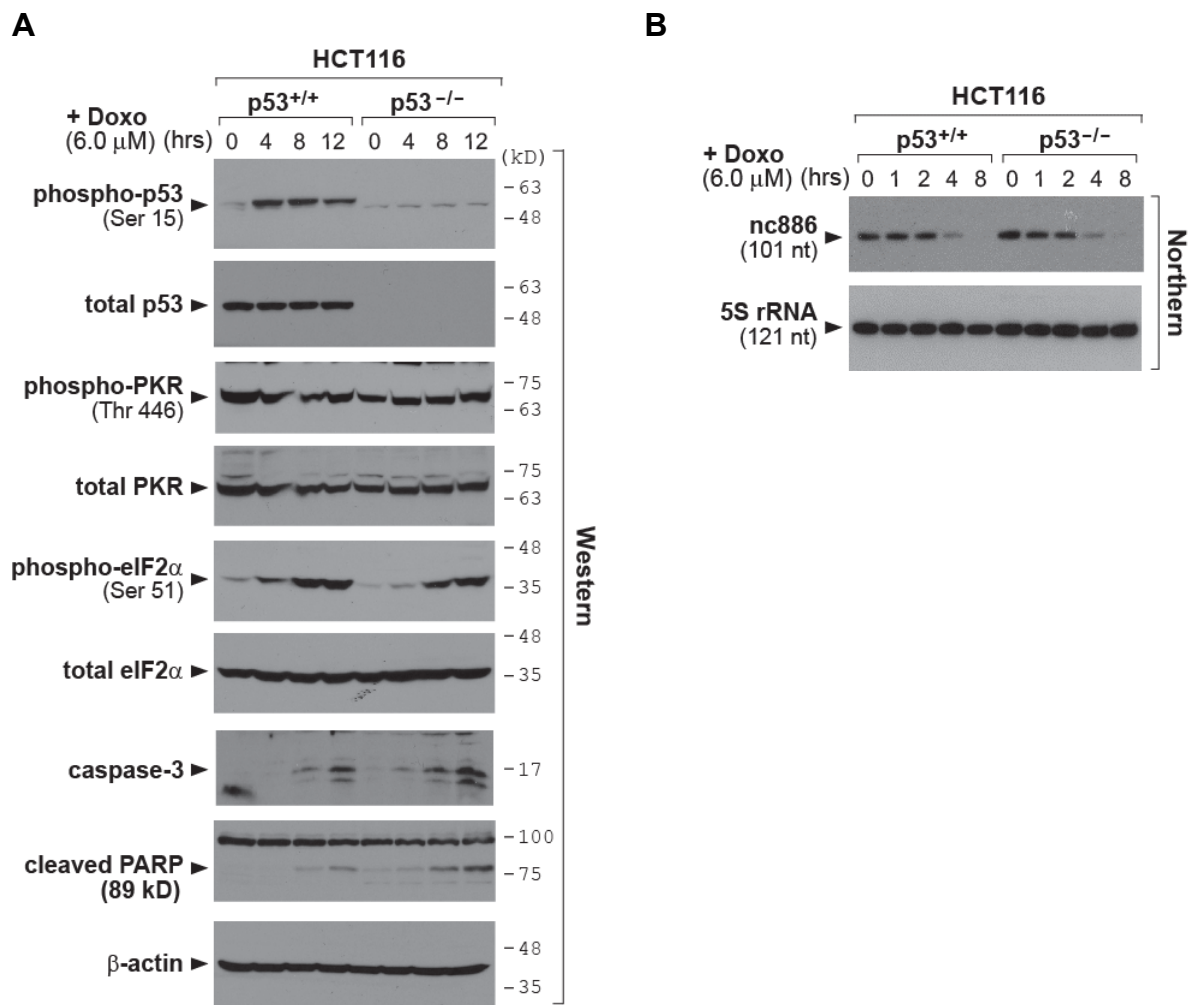


**The KD of MVP did not affect doxorubicin sensitivity**

siRNA against MVP was transfected for 48 hr, followed by cell harvest for Western blot (panel A) and then doxorubicin treatment for 24 hr and then MTT assays (panel B). All other descriptions are the same as Fig S2.

Since the vault complex is implicated in drug sensitivity [reviewed in (17)], we examined doxorubicin sensitivity upon KD of MVP (a major constituent of the vault complex). siRNA-mediated KD of MVP yielded a nearly identical dose-response curve to a control KD in Nthy-ori 3-1 cells (panel B). Together with Fig S10-S12, we conclude that the vault complex does not play a role in the doxorubicin response nor in the nc886/PKR pathway, although canonical vtRNAs are suppressed by doxorubicin.

**Figure S14**

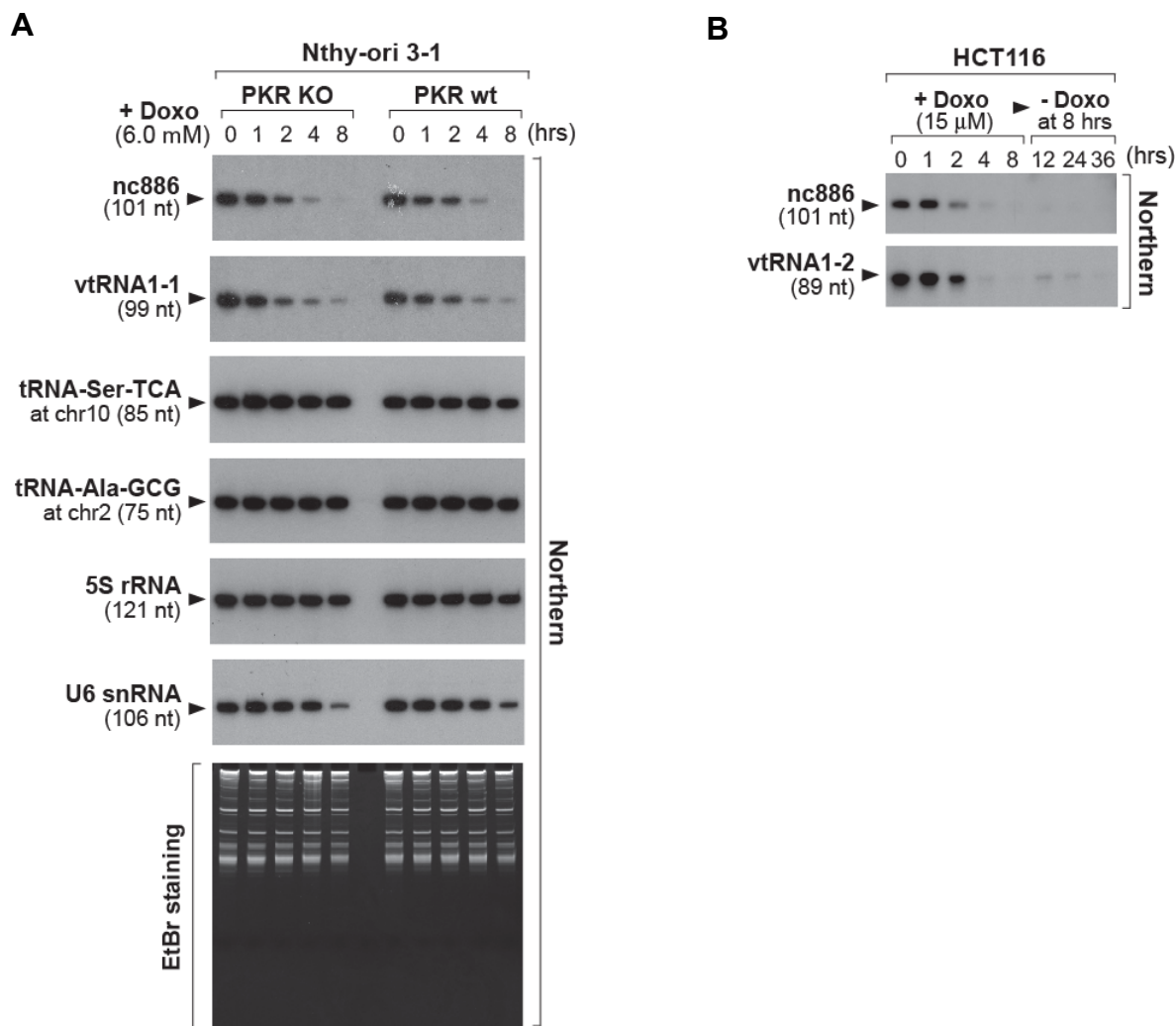


**The nc886/PKR pathway is independent of p53, although p53 has been implicated in the PKR-mediated doxorubicin cytotoxicity**

**A-B.** Western (panel A) and Northern (panel B) in HCT116 wt and p53 null cells.

In the doxorubicin-induced PKR activation, a role of p53 has been suggested but remained unclear due to conflicting results between studies (12, 13). Also, p53 is known to suppress general Pol III activity (18) and possibly influences nc886 expression. So, we wanted to clarify if p53 is involved in the nc886/PKR pathway upon doxorubicin treatment, by using p53 wt and null HCT116 cells (p53<sup>+/+</sup> and p53<sup>-/-</sup>, see p53 Western in panel A). These two cell lines had equivalent expression levels of nc886, which was suppressed by doxorubicin in a nearly identical time-course (panel B). Consequently, PKR was activated as indicated by eIF2 $\alpha$  phosphorylation, leading to apoptosis (panel A). These events occurred to a comparable extent in both cell lines. PKR levels were almost same across all the lanes, indicating that PKR was not a transcriptional target of p53 nor was induced by doxorubicin. Nonetheless, it is still a valid possibility that p53 might play a marginal role in the PKR pathway, because eIF2 $\alpha$  phosphorylation was slightly attenuated in p53<sup>-/-</sup> cells in all three studies [panel A and (12, 13)].

**Figure S15**



**Measurement of several genes transcribed by RNA polymerase III (Pol III genes)**

**A-B.** Northern blot of indicated Pol III genes. In panel A and B, nc886 Northern was reclaimed from Fig 2C and 2B respectively, for easy comparison to other Pol III genes and vtRNA1-2. EtBr staining ensures equal loading. Bands from PKR wt Nthy-ori 3-1 (the right portion of panel A) were quantified with AlphaView software 2.0.1.1 (Alpha Innotech Corp.) and normalized to the value at 0 hr, which was set as 1. The quantitation data are plotted and shown in Fig S16.

Figure S16

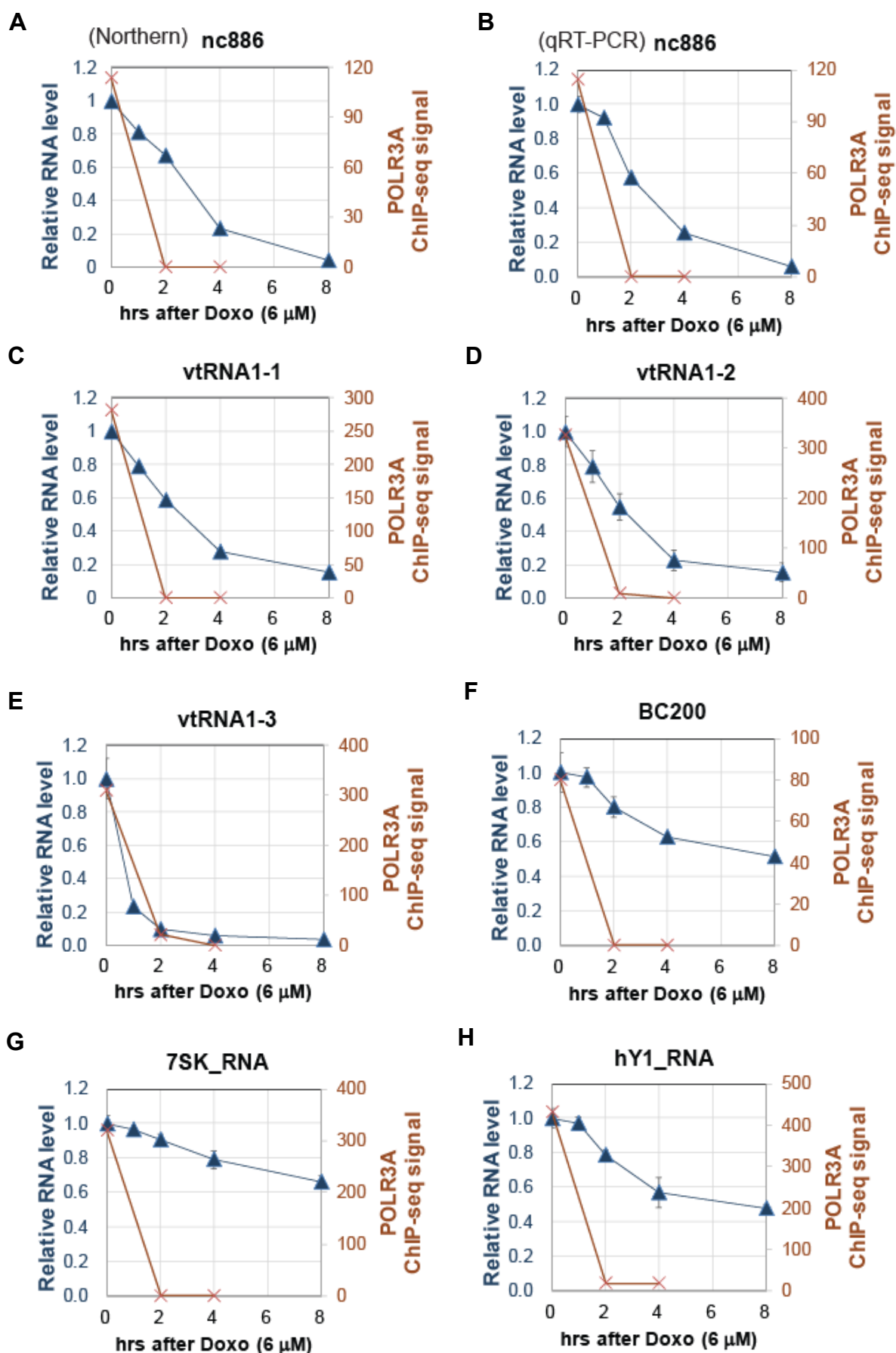


Figure S16 (continued)

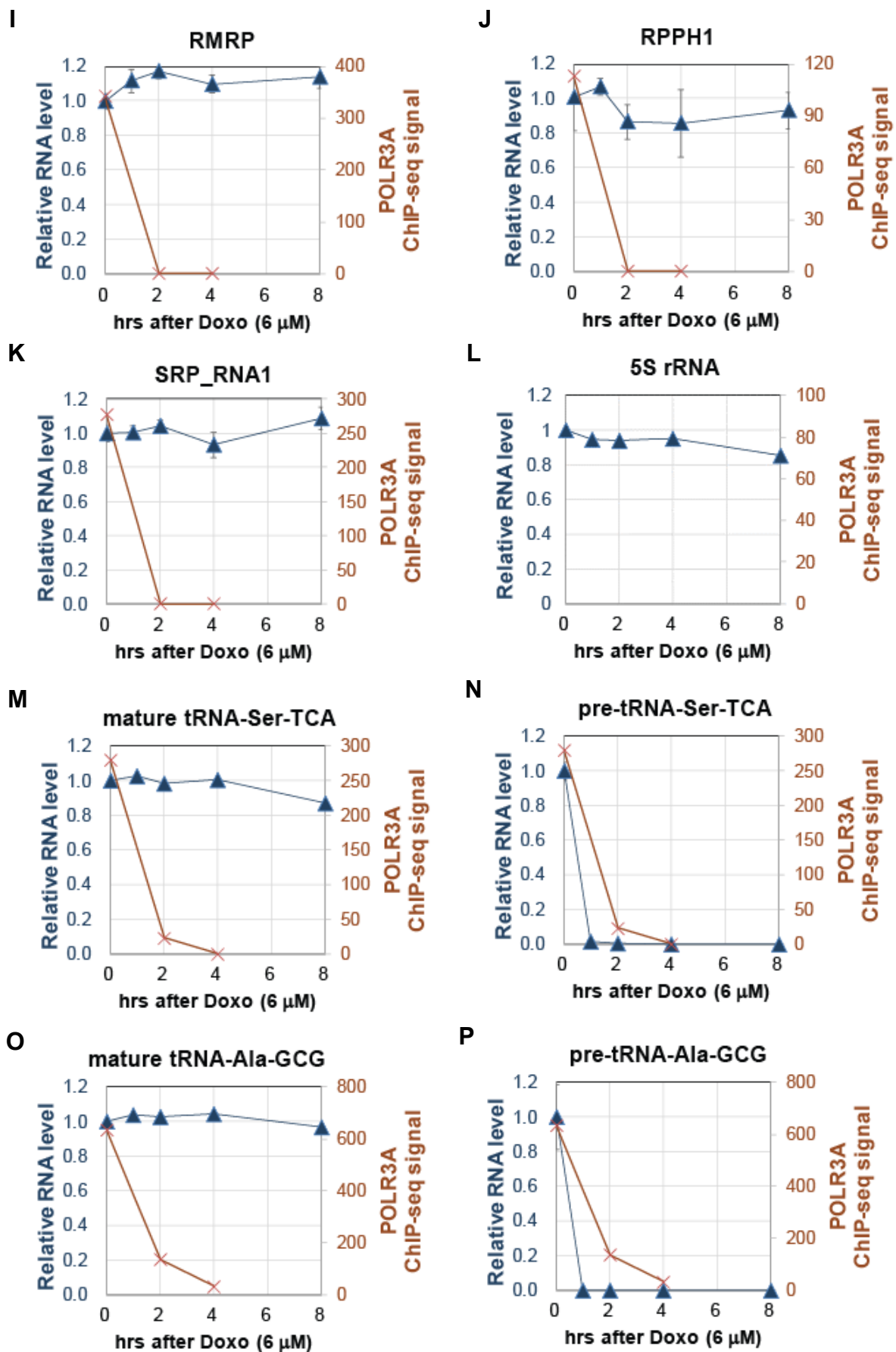
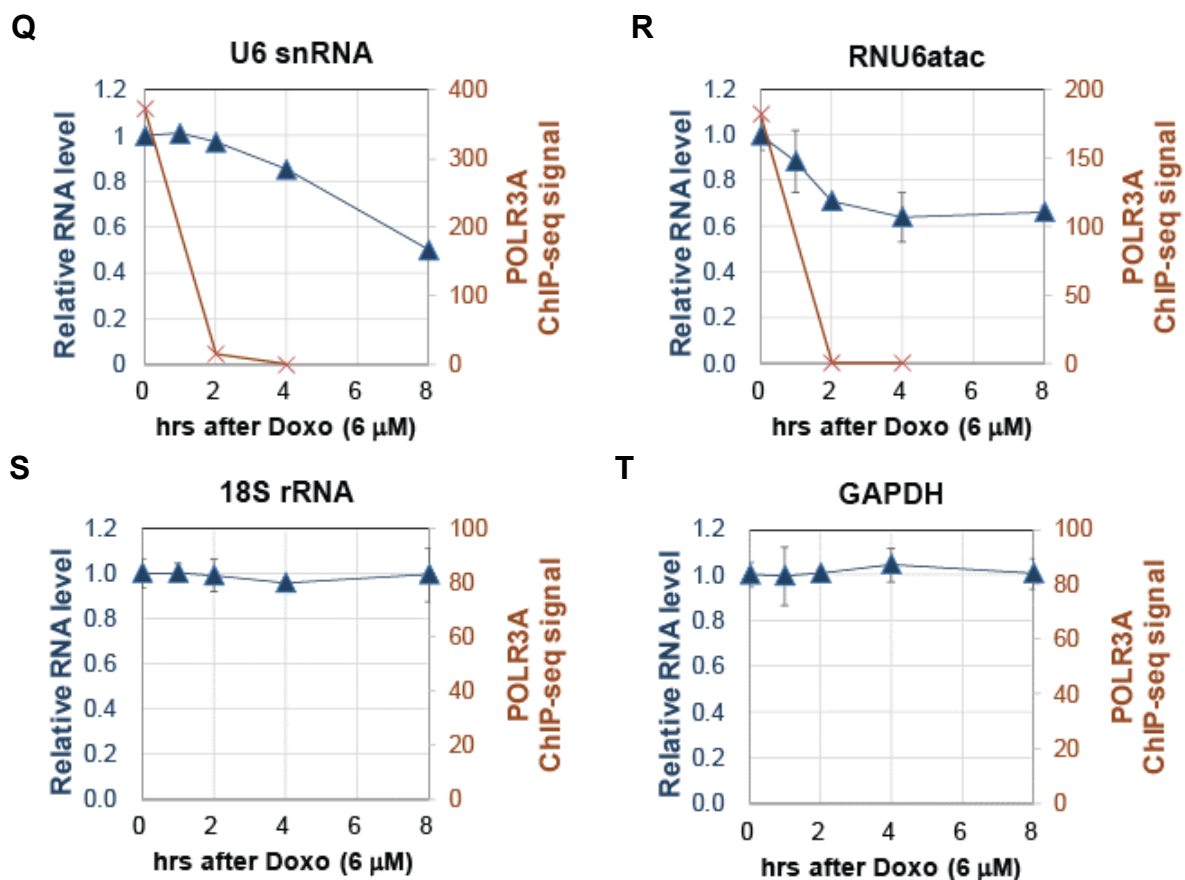


Figure S16 (continued)



### RNA expression and POLR3A ChIP-seq values of several genes transcribed by RNA polymerase III (Pol III genes)

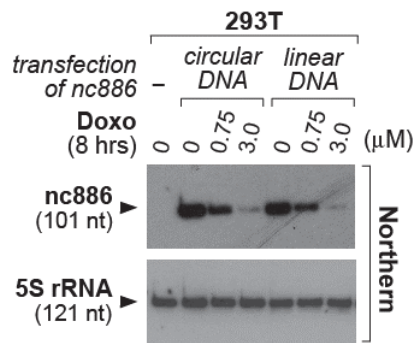
A-T. RNA expression levels were measured by Northern hybridization (for panels A, C, L, M, O, and Q; see Fig S15 for the Northern images) or qRT-PCR assays (for all the other panels). Northern hybridization was done in Nthy-ori 3-1 (from Fig S15) and qRT-PCR was done in HCT116 at 0, 1, 2, 4, 8 hrs after doxorubicin treatment. qRT-PCR values are  $2^{-\Delta C_t}$  values relative to the value at 0 hr. An average and the standard deviation were calculated from triplicate samples and plotted (blue triangles on the left axis). The data from Northern and qRT-PCR were highly consistent, as shown representatively in the case of nc886 (compare panel A-B).

POLR3A ChIP-seq was done at 0, 2, 4 hrs after doxorubicin treatment in HCT116 and peak values of each indicated gene were plotted (clay saltires on the right axis). The graph could not be drawn in the case of 18S rRNA (which is transcribed by RNA polymerase I) and GAPDH (transcribed by RNA polymerase II), because POLR3A ChIP-seq signal was absent therein. We omitted a graph also for 5S rRNA, in this case because a ChIP-seq value could not be mapped a locus due to its highly repetitive nature.

The majority of Pol III-transcribed ncRNAs did not undergo acute decrease, despite the immediate dissociation of the Pol III enzyme (POLR3A) from DNA. This tendency was the most dramatically seen when comparing panels M-P. Most of the mature tRNAs remained stable until 4-8 hrs (panels M and O), whereas POLR3A dissociation as well as transcription of the corresponding precursor tRNAs (pre-tRNAs) was almost complete within 2 hrs (panels

N and P). Pre-tRNAs are regarded as the most sensitive indicator to assess Pol III transcription rates, because they are processing intermediates and have a very short half-life. In many cases, Pol III-transcribed ncRNAs play fundamental cellular roles and are known to be stable, due to an extensive secondary structure, post-transcriptional covalent modification, or formation of tight RNA-protein complexes (19). As shown in this figure and Fig 3A, all Pol III-transcribed ncRNAs, except for nc886 and vtRNAs, remained more than half until 4 hr after doxorubicin treatment, when the PKR-dependent apoptosis was already evident (Fig 1A). Canonical vtRNAs (vtRNA1-1, 1-2, and 1-3) have been shown to have a comparable half-life to nc886 (7) and were decreased by doxorubicin with nearly identical kinetics to nc886 (panels A-E). However, vtRNAs did not play a role in doxorubicin cytotoxicity, as demonstrated in Fig S10-13. Collectively, nc886 depletion was the cause of PKR activation and consequent apoptosis, although POLR3A was dissociated and thereby general Pol III transcription was shut off immediately by doxorubicin.

**Figure S17**



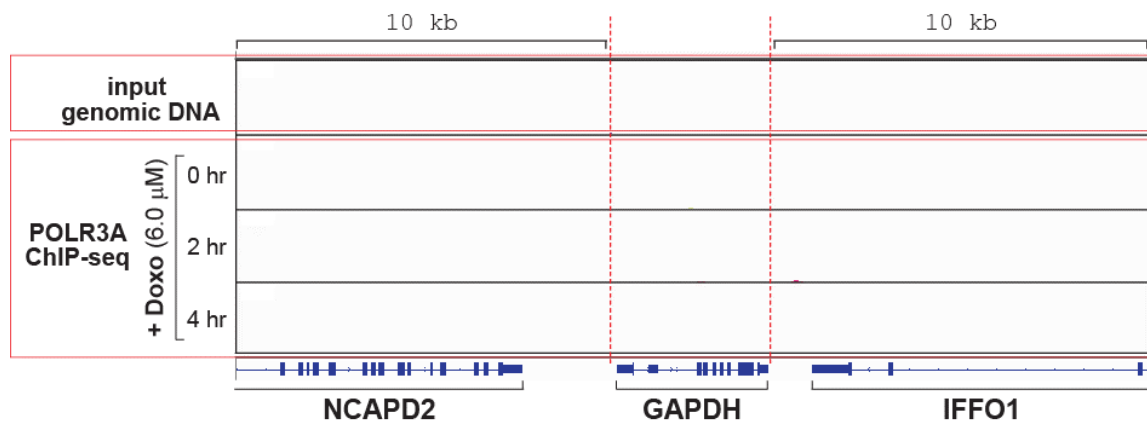
**Inhibition of Pol III transcription by doxorubicin is not due to intercalation into DNA and the resultant DNA torsion**

Northern blot of nc886 at 24 hr after transfecting a circular plasmid DNA or linear DNA expressing nc886. 293T is an nc886-silenced cell line (see lane 1) and so the signal is from exogenous nc886.

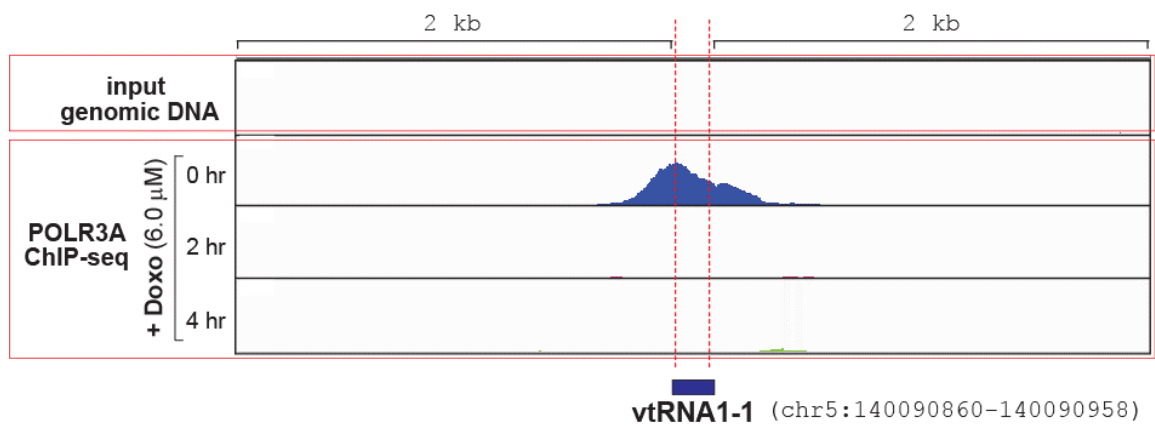
To test the mechanism for doxorubicin to suppress Pol III transcription, we compared a circular plasmid DNA with a linear DNA for nc886 expression. If the topological tension were the reason, a circular DNA would be more affected than a linear DNA. The transcription of nc886 from the two DNA templates was similarly inhibited by doxorubicin, suggesting that topological interference was an unlikely mechanism for doxorubicin to inhibit Pol III transcription.

Figure S18

A



B



C

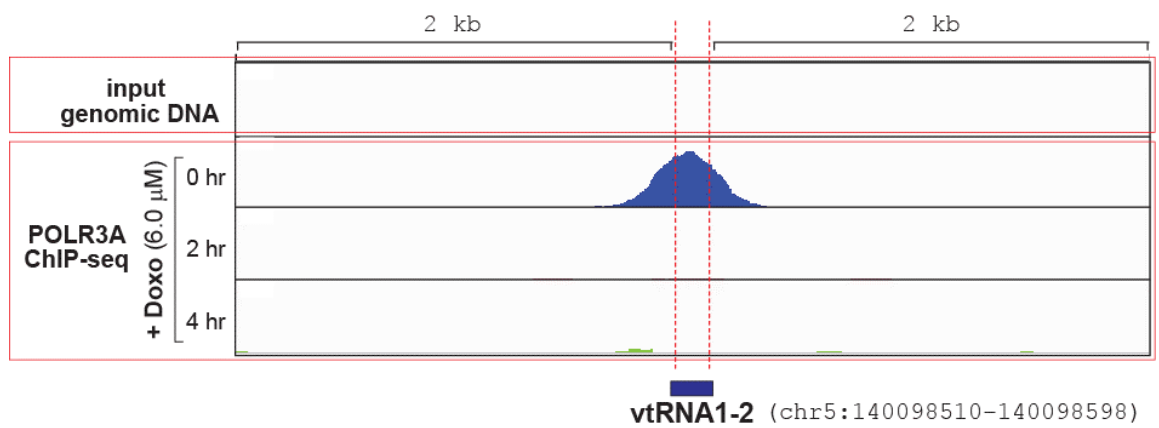
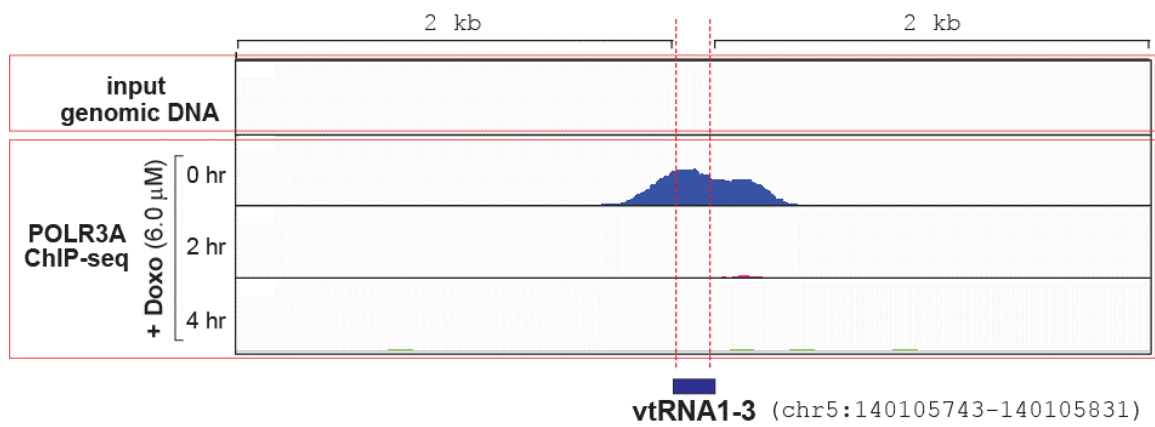
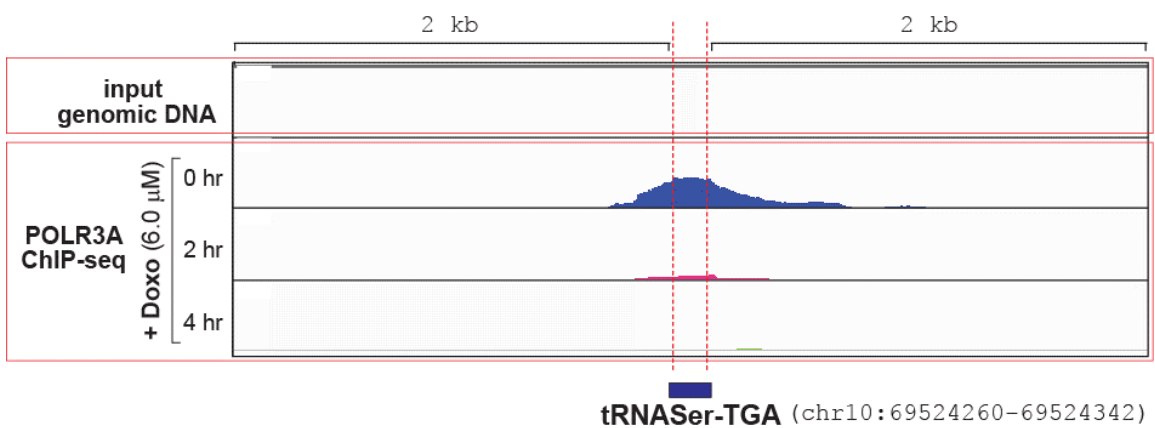


Figure S18 (continued)

D



E



F

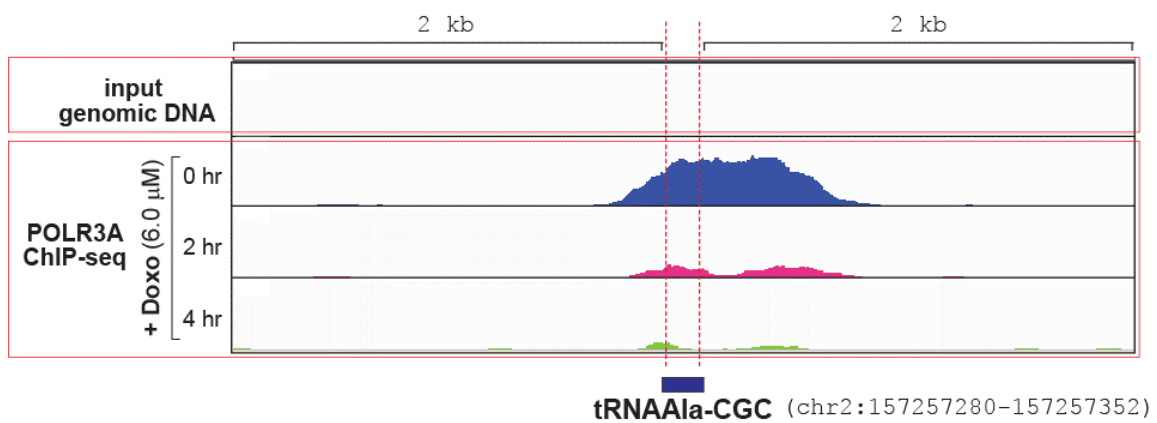
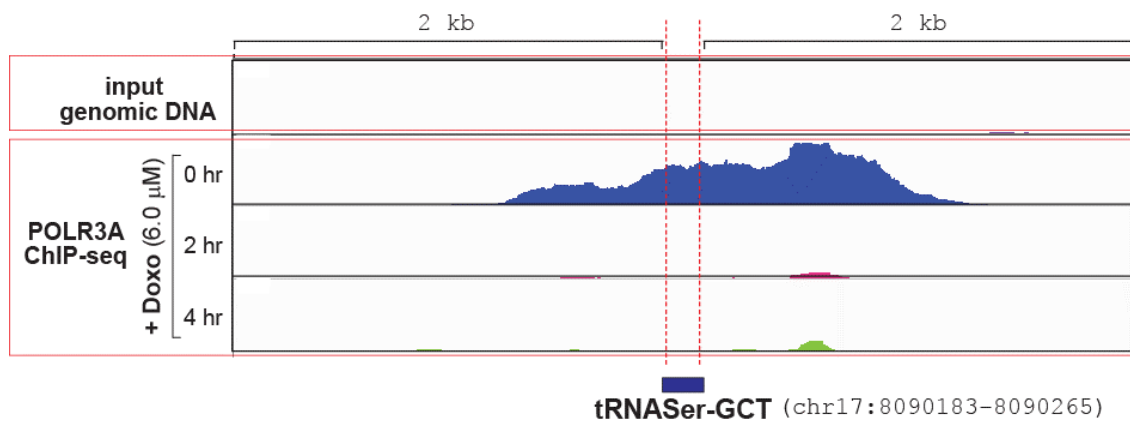
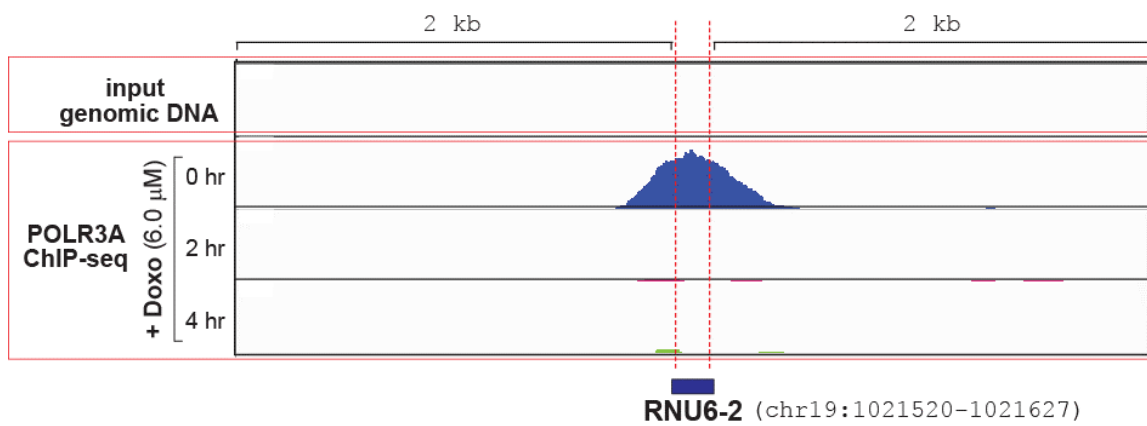


Figure S18 (continued)

G



H



I

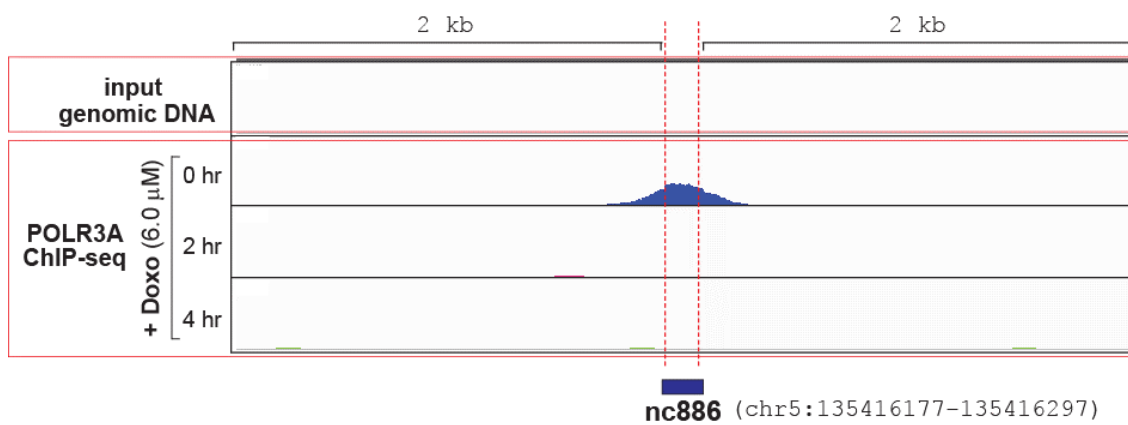


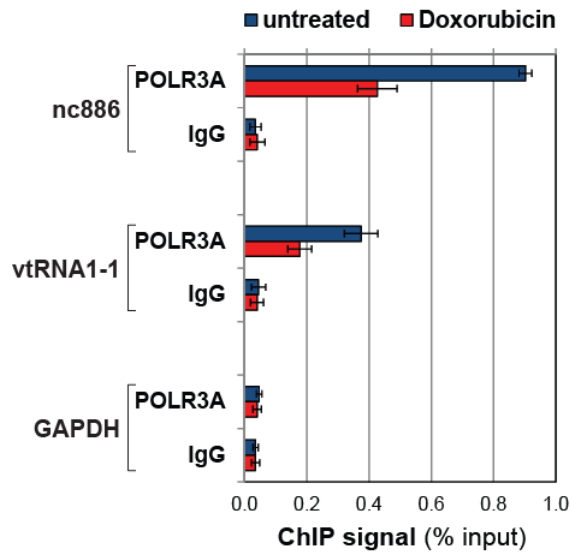
## Figure S18 (continued)

### **POLR3A ChIP-seq peaks**

**A.** Genomic visualization of a POLR3A ChIP-seq peak at the GAPDH, a gene that is transcribed by RNA polymerase II, for comparison to genes transcribed by RNA polymerase III (Pol III genes; shown in panel B-I). IGV 2.3 was used for visualization. Peaks for input DNA (before antibody precipitation) and POLR3A ChIP-DNA from three samples (0 hr is no treatment, 2 and 4 hr after doxorubicin treatment) are shown. The x-axis is the genomic coordinate (hg19) displaying the entire GAPDH gene and flanking 10 kb regions at both sides. The y-axis is the normalized ChIP-seq density and the scale was adjusted to the same as panel B-I. Under this y-axis scale, a peak was absent in any of the 0, 2, 4 hr samples.

**B-I.** Genomic visualization of POLR3A ChIP-seq peaks at several Pol III genes. All descriptions are the same as panel A, except for the x-axis that displays each gene and flanking 2 kb regions at both sides. nc886 peaks is reclaimed from Fig 3C in which the flanking 1 kb regions are shown. In all the Pol III genes shown here, peaks were located at or near the gene as expected in 0 hr sample but dramatically decreased in 2 and 4 hr samples (see also Fig S16). Together with the absence of a peak of a Pol II gene (panel A), these data assured the legitimacy of our ChIP-seq experiments and proved that doxorubicin evicts POLR3A from DNA.

Figure S19

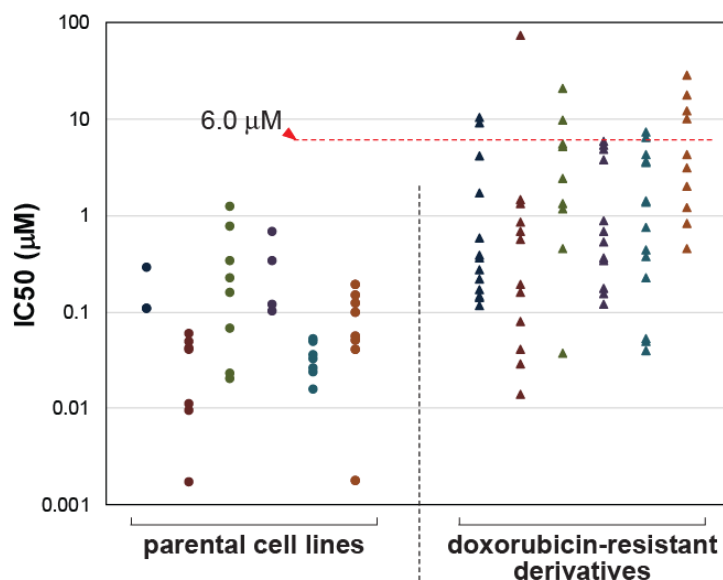


**Doxorubicin dissociates POLR3A from Pol III gene loci (nc886 and vtRNA1-1)**

qPCR of indicated genomic regions bound to POLR3A, after treatment of 6  $\mu$ M doxorubicin for 2 hr.  $2^{-\Delta C_t}$  values from POLR3A and IgG ChIP DNA were normalized to input DNA to calculate fold-enrichment (y-axis). The measurement was in triplicates.

POLR3A bound to nc886 and vtRNA1-1, but not to a GAPDH locus; the POLR3A binding to both loci was significantly decreased by doxorubicin.

Figure S20



**The IC<sub>50</sub> values of doxorubicin-resistant cell lines derived from their doxorubicin-sensitive cells, as compared to our treatment condition 6  $\mu\text{M}$**

A dot plot of IC<sub>50</sub> values of parental cells (circles on the left) and their doxorubicin-derivatives (triangles on the right) that were collected from 26 papers (see SI Appendix, Dataset S3 for full information). To avoid data points to be too crowded, we classified them according to tissue origins and displayed in different colors: dark blue (breast), red (central nervous system), olive green (gastrointestinal tract), purple (lung), aqua (ovary and prostate), and orange (others including blood, bone, liver, uterine, and bladder).

A major problem in chemotherapy is the appearance of drug-resistant cells and, as a consequence, the recurrence of malignancies. In a number of reports, such resistant cells have been *in vitro* developed with gradually increasing drug concentrations or isolated from recurring tumors in patients after chemotherapy. We did a literature survey, collected IC<sub>50</sub> values from parental cells and their doxorubicin-resistant derivatives, and found that all parental cells (38 out of 38) and the majority of cells in the doxorubicin-resistant group (60 out of 71; 84.5 %) had IC<sub>50</sub> < 6  $\mu\text{M}$ . These data suggest that our treatment condition (at 6  $\mu\text{M}$  for 30 min) could be largely effective also in recurrent tumors.

## Supplementary References

1. Lee K, *et al.* (2011) Precursor miR-886, a novel noncoding RNA repressed in cancer, associates with PKR and modulates its activity. *RNA* 17(6):1076-1089.
2. Kunkeaw N, *et al.* (2013) Cell death/proliferation roles for nc886, a non-coding RNA, in the protein kinase R pathway in cholangiocarcinoma. *Oncogene* 32(32):3722-3731.
3. Lee EK, *et al.* (2016) nc886, a non-coding RNA and suppressor of PKR, exerts an oncogenic function in thyroid cancer. *Oncotarget* 7(46):75000-75012.
4. Kim Y, *et al.* (2018) PKR Senses Nuclear and Mitochondrial Signals by Interacting with Endogenous Double-Stranded RNAs. *Mol. Cell* 71(6):1051-1063 e1056.
5. Kickhoefer VA, *et al.* (1998) Vaults are up-regulated in multidrug-resistant cancer cell lines. *J. Biol. Chem.* 273(15):8971-8974.
6. Park K, *et al.* (2012) Transcriptional activation of the IL31 gene by NFAT and STAT6. *J. Leukoc. Biol.* 91(2):245-257.
7. Park JL, *et al.* (2017) Epigenetic regulation of RNA polymerase III transcription in early breast tumorigenesis. *Oncogene* 36(49):6793-6804.
8. Bennett RL, *et al.* (2012) Increased expression of the dsRNA-activated protein kinase PKR in breast cancer promotes sensitivity to doxorubicin. *PLoS One* 7(9):e46040.
9. Cheng X, Bennett RL, Liu X, Byrne M, & Stratford May W (2013) PKR negatively regulates leukemia progression in association with PP2A activation, Bcl-2 inhibition and increased apoptosis. *Blood cancer journal* 3:e144.
10. Peidis P, Papadakis AI, Muaddi H, Richard S, & Koromilas AE (2011) Doxorubicin bypasses the cytoprotective effects of eIF2alpha phosphorylation and promotes PKR-mediated cell death. *Cell Death Differ.* 18(1):145-154.
11. Tu YC, *et al.* (2012) Blocking double-stranded RNA-activated protein kinase PKR by Japanese encephalitis virus nonstructural protein 2A. *J. Virol.* 86(19):10347-10358.
12. Yoon CH, Lee ES, Lim DS, & Bae YS (2009) PKR, a p53 target gene, plays a crucial role in the tumor-suppressor function of p53. *Proc. Natl. Acad. Sci. U. S. A.* 106(19):7852-7857.
13. Rahman M, Lem C, Muaddi H, & Koromilas AE (2009) PKR is not a universal target of tumor suppressor p53 in response to genotoxic stress. *Cell Cycle* 8(21):3606-3607.
14. Lee KS, *et al.* (2014) nc886, a non-coding RNA of anti-proliferative role, is suppressed by CpG DNA methylation in human gastric cancer. *Oncotarget* 5(11):3944-3955.
15. Lee HS, *et al.* (2014) Epigenetic silencing of the non-coding RNA nc886 provokes oncogenes during human esophageal tumorigenesis. *Oncotarget* 5(11):3472-3481.
16. Stadler PF, *et al.* (2009) Evolution of vault RNAs. *Mol. Biol. Evol.* 26(9):1975-1991.
17. van Zon A, Mossink MH, Scheper RJ, Sonneveld P, & Wiemer EA (2003) The vault

- complex. *Cell. Mol. Life Sci.* 60(9):1828-1837.
18. Marshall L & White RJ (2008) Non-coding RNA production by RNA polymerase III is implicated in cancer. *Nat. Rev. Cancer* 8(12):911-914.
  19. Turowski TW & Tollervey D (2016) Transcription by RNA polymerase III: insights into mechanism and regulation. *Biochem. Soc. Trans.* 44(5):1367-1375.